

---

# Design of Compressed Sensing Systems via Density-Evolution Framework for Structure Recovery in Graphical Models

---

Muralikrishna G. Sethuraman<sup>1</sup> Hang Zhang<sup>1</sup> Faramarz Fekri<sup>1</sup>

## Abstract

It has been shown that the task of learning the structure of Bayesian networks (BN) from observational data is an NP-Hard problem. Although there have been attempts made to tackle this problem, these solutions assume direct access to the observational data which may not be practical in certain applications. In this paper, we explore the feasibility of recovering the structure of Gaussian Bayesian Network (GBN) from compressed (low dimensional and indirect) measurements. We propose a novel density-evolution based framework for optimizing compressed linear measurement systems that would, by design, allow for more accurate retrieval of the covariance matrix and thereby the graph structure. In particular, under the assumption that both the covariance matrix and the graph are sparse, we show that the structure of GBN can indeed be recovered from resulting compressed measurements. The numerical simulations show that our sensing systems outperform the state of the art with respect to Maximum absolute error (MAE) and have comparable performance with respect to precision and recall, without any need for ad-hoc parameter tuning.

## 1. Introduction

Graph structure recovery has been a problem of interest in the last few decades within the machine learning community. It is well known that structure recovery is an NP-hard problem, (Chickering et al., 2004), and in general it cannot be uniquely identified (Guo et al., 2020). Nevertheless, attempts have been made to recover the structure of the graphical model under various assumptions on the underlying probability distribution governing the system. *Additive Noise Models* (ANM) have gained a lot of traction in the recent years due to its analytic simplicity and has been shown

that in such a case the graph structure can be uniquely identified. In particular, (Ghoshal & Honorio, 2017) showed that when the additive noise is Gaussian, the structure of the Gaussian Bayesian Network (GBN) can be recovered in polynomial time.

However, aforementioned solutions assume direct access to the observational data which may not be practical in certain applications (Müller et al., 2008), making it an expensive task to recover the structure of the underlying graph, especially in high dimensions. In this work we study the feasibility of recovering the structure of directed graph for the case when the additive noise is Gaussian distributed. In particular, we are interested in recovering the graph structure by collecting observations through a linear measurement system of the form,

$$\mathbf{y} = \mathbf{A}\mathbf{x} + \mathbf{n},$$

where  $\mathbf{y}$  is of a lower dimension than  $\mathbf{x}$ , where  $\mathbf{x}$  is the random vector whose components are the nodes of the GBN. The crux of our approach relies on *density evolution* analysis of *message-passing* algorithm, also known as *Belief propagation*, *min-product* or *max-sum*. The algorithm was independently developed in different fields in the last century. In 1935, Bethe (Mezard & Montanari, 2009) used it to approximately compute the partition function. Pearl developed belief propagation in 1988 to perform exact inference in Acyclic Bayesian Networks, (Pearl, 1988).

**Related Work.** Structure recovery methods for directed graphs can broadly be divided into two categories: (1) Independence test based, and (2) score based methods. Independence test based methods (Spirtes et al., 2000) typically involve computing the conditional independence between any two nodes in the graph conditioned on all the subsets of the remaining nodes. These methods are computationally intensive as the total number of independence tests to be performed grows exponential in the size of the graph. Moreover, these methods are only capable of finding the graph structure upto Markov equivalency.

On the other hand, score based methods rely on a metric to score the candidate *directed acyclic graph* (DAG) based on how well it explains the data. Popular examples of scores are *Akaike Information Criterion* (AIC), Bayesian Informa-

---

<sup>1</sup>School of Electrical and Computer Engineering, Georgia Institute of Technology, Atlanta, USA. Correspondence to: Muralikrishna G. Sethuraman <muralikgs@gatech.edu>.

tion Criterion (BIC) and  $\ell_0$  penalized log-likelihood score by (Van de Geer & Bühlmann, 2013). A combinatorial search over the entire space of DAGs is still expensive as the size grows exponentially with number of node in the graph. (Zheng et al., 2018) proposed a continuous constraint to restrict the search space to that of DAGs using the weighted adjacency matrix and showed its effectiveness for the case of ANM, but they're overall optimization program is non-convex and hence not easy to analyze. (Ghoshal & Honorio, 2017) showed that for ANMs that are also GBNs, the graph structure can be recovered in polynomial time. These are only a few examples from the vast literature available for structure learning, for more information we refer the interested reader to (Guo et al., 2020).

Sparse vector recovery from compressed measurements has been studied quite extensively with several sensing matrices being proposed in the literature (Candes et al., 2006; DeVore, 2007; Kaplan et al., 2018), each offering a several advantages over the others. Overtime, Gaussian sensing matrices have become a popular choice for sparse vector recovery. However, (Kaplan et al., 2018) showed that gaussian sensing matrix is not a very good candidate for recovery of sparse matrices. (Berinde et al., 2008) showed the use of binary matrices, in particular adjacency of  $\delta$ -left regular bipartite graph for sparse vector recovery. (Dasarathy et al., 2015) built upon the work done (Berinde et al., 2008) and proved that adjacency of  $\delta$ -left regular bipartite graphs can be used for recovery of sparse matrices.

Finally, in the 1960s (Gallager, 1962) proposed sum-product algorithm to decode *low-density parity check* (LDPC) codes over graphs, which was forgotten for decades and later reinvented along with density evolution to design LDPC codes achieving channel capacity. (Krzakala et al., 2012a;b; Zdeborová & Krzakala, 2016) analyzed the a sparse sensing matrix based on spatial coupling using DE for sparse vector recovery. (Zhang et al.) employed density evolution and developed a framework for designing sensing matrices for regular as well as preferential recovery of sparse vectors. For better understanding of usage of message passing and density evolution for signal recovery we again refer the readers to (Mezard & Montanari, 2009; Zdeborová & Krzakala, 2016).

**Contributions.** This work is the first application of density evolution and message passing algorithms in the problem of structure recovery of graphical models. In particular, our focus is on Gaussian Bayesian Networks (GBN) with sparse covariance matrix and sparse precision matrix, i.e., the number of edges in the graph is small compared to a fully connected network. To the best of our knowledge this is the first work to consider recovery of structure of GBN from compressed (indirect) measurements. We summarize our contributions as follows:

1. We propose a novel approach to optimally design a low dimensional data collection (measurement) scheme from a high dimensional signal that would allow for recovering sparse covariance matrix from these measurements. We use density evolution based analysis of message-passing algorithm to reduce the design procedure into a convex program.
2. Through numerical simulations we showcase the effectiveness of our proposed sensing systems for recovery of covariance matrix and the structure of the GBN. Our method outperforms the current state of the art with respect to *Maximum Absolute Error* (MAE), which measures the maximum difference between the ground truth and the estimated covariance matrix. We also show that the compressed achievable increases with the size of the graph.

**Organization.** In section 2 we describe the covariance and the structure recovery problem, followed by a description of the steps involved in designing the sensing system for covariance recovery via density evolution is section 3. In section 4 we discuss the recovery of GBN structure from the covariance and the precision matrix. We showcase the effectiveness of our approach via numerical simulations in section 5 and end with conclusion in section 6.

## 2. Problem Description

In this section we provide a formal description of our problem starting with the notations.

**Notations.** All vectors are denoted by lowercase boldface letters,  $\mathbf{x}$  and matrices by uppercase boldfaced letters,  $\mathbf{A}$ .  $\mathbf{A}_{*,i}$  denotes the  $i$ -th column of the matrix  $\mathbf{A}$ , similarly  $\mathbf{A}_{j,*}$  denotes the  $j$ -th row of  $\mathbf{A}$ .  $\|\mathbf{A}\|_1 = \sum_{ij} |A_{ij}|$  and  $\|\mathbf{A}\|_F = \sqrt{\sum_{ij} A_{ij}^2}$  and  $\|\mathbf{x}\|_p = (\sum_i x_i^p)^{1/p}$ .

A Gaussian Bayesian Network (GBN) is a graph  $G = (V, E)$  where the parent-child relationship between the nodes is represented by a DAG and the child nodes are Gaussian distributed given the parents. Let  $X_i$  represent the random variable corresponding to the  $i^{th}$  node in the  $G$ ,  $\mathbf{x} = (X_1, \dots, X_p)$  be a vector with the nodes of  $G$  as its components. A GBN can equivalently be viewed using a *linear structural equation model* (SEM) as follows,

$$X_i = \mathbf{W}_{*,i}^T \mathbf{x} + Z_i \quad (1)$$

where  $\mathbf{W}$  is the weighted adjacency matrix of  $G$  ( $W_{ij}$  is the weight corresponding to the edge going from  $X_i$  to  $X_j$ ), and  $Z_i \sim \mathcal{N}(0, \sigma^2)$ . This would imply that  $\mathbf{x} \sim \mathcal{N}(0, \Sigma)$ , where

$$\Sigma = \sigma^2 (\mathbf{I} - \mathbf{W}^T)^{-1} (\mathbf{I} - \mathbf{W}^T)^{-T}. \quad (2)$$

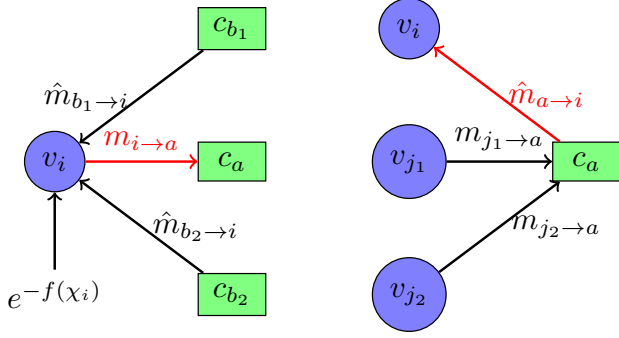


Figure 1. Illustration of flow of messages in the factor graph. The blue circles denote the variable nodes and the check nodes are depicted as the green rectangular nodes.

The covariance matrix ( $\Sigma$ ) and inverse covariance (precision) matrix ( $\Omega$ ) uniquely identify the distribution.

We now pass this through a linear measurement system,

$$\mathbf{y} = \mathbf{A}\mathbf{x} + \mathbf{n},$$

where  $\mathbf{y} \in R^d$ ,  $\mathbf{x} \in R^p$ ,  $\mathbf{A} \in R^{d \times p}$ , and  $\mathbf{n} \in R^d$  and  $\mathbf{y}$ ,  $\mathbf{A}$ ,  $\mathbf{n}$  denote the observations, sensing matrix and the measurements noise respectively. Consider the case where  $d < p$ , we are interested in the problem of recovering the graph structure  $G = (V, E)$  from the observations  $\mathbf{y}$ . In particular, we wish to optimize the sensing matrix  $\mathbf{A}$  that would provide a more accurate structure recovery.

It has been shown that, (Ghoshal & Honorio, 2017), from knowing the covariance ( $\Sigma$ ) and precision matrix ( $\Omega$ ) it is possible to recover the underlying GBN structure, see section (4) for more details. Therefore, our problem boils down to recovering the covariance ( $\Sigma$ ) and precision matrix ( $\Omega$ ) from the observations  $\mathbf{y}$ , i.e., the low dimensional projection of  $\mathbf{x}$ .

### 3. Covariance Recovery

Under the linear measurement system discussed in the previous section, when the measurement noise is zero, the covariance of the observations  $\mathbf{y}$  is given by

$$\Sigma_Y = \mathbf{A}\Sigma\mathbf{A}^T. \quad (3)$$

We further make the assumption that the covariance of  $X$  is a sparse matrix. The covariance recovery can now be posed as the following convex program,

$$\begin{aligned} \min_{\Sigma} \quad & \|\Sigma\|_1 \\ \text{subject to} \quad & \Sigma_Y = \mathbf{A}\Sigma\mathbf{A}^T \end{aligned} \quad (\text{P}_1)$$

Since we only have access to the observed samples of  $\mathbf{y}$ , the true covariance is approximated by the sample covari-

ance,  $\Sigma_Y^{(N)} = (1/N) \sum_i \mathbf{y}_i \mathbf{y}_i^T$ , and hence (P<sub>1</sub>) is relaxed as follows

$$\begin{aligned} \min_{\Sigma} \quad & \|\Sigma\|_1 \\ \text{subject to} \quad & \left\| \Sigma_Y^{(N)} - \mathbf{A}\Sigma\mathbf{A}^T \right\|_F^2 \leq \kappa \end{aligned} \quad (\text{P}_2)$$

Upon vectorization, we have  $\mathbf{A}\Sigma\mathbf{A}^T = (\mathbf{A} \otimes \mathbf{A})\text{vec}(\Sigma)$ , where  $\otimes$  denotes the Kronecker product. This gives the following equivalent formulation of (P<sub>2</sub>),

$$\begin{aligned} \min_{\Sigma} \quad & \|\text{vec}(\Sigma)\|_1 \\ \text{subject to} \quad & \left\| \text{vec}(\Sigma_Y^{(N)}) - (\mathbf{A} \otimes \mathbf{A})\text{vec}(\Sigma) \right\|_2^2 \leq \kappa \end{aligned} \quad (\text{P}_2)$$

In this vectorized form,  $(\mathbf{A} \otimes \mathbf{A})$  can be thought of as the new sensing matrix having a Kronecker product structure and  $\text{vec}(\Sigma)$  to be the sparse vector that has to be recovered.

#### 3.1. Design of Sensing Matrix using Density Evolution

For ease of notation let us denote  $\gamma = \text{vec}(\Sigma_Y)$ ,  $\chi = \text{vec}(\Sigma)$ , and  $\mathbf{A}^\otimes = \mathbf{A} \otimes \mathbf{A}$ . Following (Zhang et al.), the solution to (P<sub>2</sub>) can be viewed as the solution to the following *maximum a posteriori* (MAP) estimator

$$\hat{\chi} = \arg \max_{\chi} \exp \left( -\frac{\|\gamma - \mathbf{A}^\otimes \chi\|_2^2}{2\sigma^2} \right) \exp(-f(\chi)), \quad (4)$$

where  $f(\chi)$  is the generalized regularizer term. When  $f(\chi)$  is set to  $\|\chi\|_1$  then the MAP estimator is exactly equivalent to (P<sub>2</sub>). Here, we make a few assumptions on the sensing matrix and the regularizer:

1. The sensing matrix  $\mathbf{A}$  is sparse with  $E A_{ij} = 0$  and  $A_{ij} \in \{0, \pm A^{-1/2}\}$ .
2. The regularizer  $f(\chi)$  can be decomposed,  $f(\chi) = \sum_i f(\chi_i)$ .

To develop the density evolution framework, we associate (4) with a factor graph  $\mathcal{G} = (\mathcal{V}, \mathcal{E})$  consisting of nodes corresponding to components of  $\chi$  (variable nodes) and components of  $\gamma$  (check nodes), see Figure 3. An edge exists between  $\chi_i$  and  $\gamma_j$  if  $A_{ij}^\otimes \neq 0$ .

At this point it is important to illustrate some of the key structural properties of the factor graph that arises due to the Kronecker product nature of  $\mathbf{A}^\otimes$ , see Figures 2 & 3. The check nodes and the variable nodes consists of  $d$  and  $p$  blocks respectively, and each check node block contains  $d$  nodes and each variable node block contains  $p$  nodes.  $i$ -th check node block is said to be connected to  $j$ -th variable node block if any node in the  $i$ -th check node block is connected to any node in the  $j$ -th variable node block. This

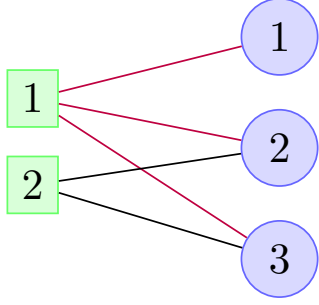


Figure 2. Illustration of the connections in factor graph corresponding to the Kronecker product when the sensing matrix is given by equation 5. The number within the node correspond to the block ID and as seen in the figure, the connections at the block level is governed by  $A$ . The check node blocks are depicted as green rectangles and the variable node blocks are depicted as blue circles.

is true when  $A_{ij} \neq 0$ . The connection between the nodes in the  $i$ -th check node block and  $j$ -th variable node block, if it exists, is determined by  $A$ . That is, within in the blocks, the  $k$ -th check node is connected to  $l$ -th variable node if  $A_{kl} \neq 0$ . Figure 3 shows the factor graph for the following sensing matrix,

$$A = \begin{bmatrix} 1 & 1 & 1 \\ 0 & 1 & 1 \end{bmatrix} \quad (5)$$

In view of the graphical model, recovery of  $\Sigma_X$  can be thought of as an inference problem over the factor graph which can be solved using message-passing algorithm. Following the notations of (Zhang et al.), let  $m_{i \rightarrow a}^{(t)}$  denote the message going from the  $i$ -th variable node to the  $a$ -th check node at the  $t$ -th iteration. Similarly, let  $\hat{m}_{a \rightarrow i}^{(t)}$  denote the message going from  $a$ -th check node to the  $i$ -th variable node at the  $t$ -th iteration, Figure 1. The message-passing algorithm is then given by

$$m_{i \rightarrow a}^{(t+1)}(\chi_i) \cong e^{-f(\chi_i)} \prod_{b \in \partial i \setminus a} \hat{m}_{b \rightarrow i}^{(t)}(\chi_i); \quad (6)$$

$$\hat{m}_{a \rightarrow i}^{(t+1)}(\chi_i) \cong \int \prod_{j \in \partial a \setminus i} m_{j \rightarrow a}^{(t+1)}(\chi_j) e^{-\frac{(\gamma_a - \sum_j A_{aj} \chi_j)^2}{2\sigma^2}} d\chi_j, \quad (7)$$

where  $\partial a$ ,  $\partial i$  denote the neighborhood of the  $a$ -th check node and the  $i$ -th variable node respectively and  $\cong$  denotes equality upto a normalization constant. At iteration  $t$ ,  $\chi_i$  can be recovered by taking argmax of the product of all the messages coming to the  $i$ -th variable node.

To aid in the design of the sensing matrix, we need to characterize the degree distribution of the variable and check nodes. In (Zhang et al.), the generating polynomials  $\lambda(\alpha) = \sum_i \lambda_i \alpha^{i-1}$  and  $\rho(\alpha) = \sum_i \rho_i \alpha^{i-1}$  are defined as the degree distributions of the variable and check nodes respectively. In our case, direct modeling of the node degree

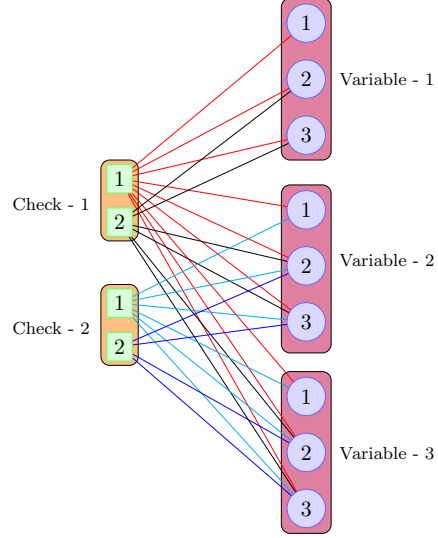


Figure 3. Illustration of the connections in the factor at the node level. The green rectangles denote the check nodes and blue circles denote the variable nodes. Due to the Kronecker product nature of the  $A \otimes A$ , the connections at node level has an elegant structure. The connections between check node block  $i$  and variable node block  $j$ , if it exists, is again governed by  $A$ .

distribution is tricky due to the Kronecker product structure of  $A^{\otimes}$ . We instead define  $\lambda(\alpha)$  and  $\rho(\alpha)$  to be the distribution of number of non zero entries in the columns and rows of  $A$ . The degree distribution of the check nodes and the variable nodes can then be obtained from  $\lambda(\alpha)$  and  $\rho(\alpha)$ , refer to appendix for more details.

### 3.1.1. DENSITY EVOLUTION

In order to design sensing matrix using *density evolution* (DE), the reconstruction of  $\Sigma$  has to be analyzed. To that end, the messages are treated as random variables and in particular they are chosen to be Gaussian distributed due to its simplicity. That is,  $m_{i \rightarrow a}^{(t)} \sim \mathcal{N}(\mu_{i \rightarrow a}^{(t)}, v_{i \rightarrow a}^{(t)})$  and  $\hat{m}_{a \rightarrow i}^{(t)} \sim \mathcal{N}(\hat{\mu}_{a \rightarrow i}^{(t)}, \hat{v}_{a \rightarrow i}^{(t)})$ . To analyze the convergence of (4) we track the following two quantities

$$E^{(t)} = \frac{1}{d^2 p^2} \sum_{a=1}^{d^2} \sum_{i=1}^{p^2} \left( \mu_{i \rightarrow a}^{(t)} - \chi_i \right)^2; \quad (8)$$

$$V^{(t)} = \frac{1}{d^2 p^2} \sum_{a=1}^{d^2} \sum_{i=1}^{p^2} v_{i \rightarrow a}^{(t)}. \quad (9)$$

Where  $E^{(t)}$  and  $V^{(t)}$  represent the average error and variance at iteration  $t$ . To enforce sparsity, the regularization function  $f(\chi)$  is set as  $\beta \|\chi\|_1$ , this is equivalent to enforcing Laplacian prior on  $\chi$ . From DE analysis for the chosen prior, the average error and variance reduce to the following



form,

$$E^{(t+1)} = \mathbf{E}_{\text{prior}(s)} \mathbf{E}_{z \sim \mathcal{N}(0,1)} \left[ \text{prox} \left( s + a_1 z \sqrt{E^{(t)}}; \beta a_2 V^{(t)} \right) - s \right]^2 \quad (10)$$

$$V^{(t+1)} = \mathbf{E}_{\text{prior}(s)} \mathbf{E}_{z \sim \mathcal{N}(0,1)} \left[ \beta a_2 V^{(t)} \text{prox}' \left( s + a_1 z \sqrt{E^{(t)}}; \beta a_2 V^{(t)} \right) \right]^2, \quad (11)$$

where  $a_1$  is given by  $\sum_{i,i',j,j'} \rho_i \rho_{i'} \lambda_j \lambda_{j'} \sqrt{i i' / j j'}$  and  $a_2$  is given by  $\sum_{i,i',j,j'} \rho_i \rho_{i'} \lambda_j \lambda_{j'} (i i' / j j')$ . Also,  $\text{prox}(a; b)$  denotes the soft-threshold function and  $\text{prox}'(a; b)$  is the derivative of the soft-threshold function with respect to the first argument. For a detailed derivation of these quantities please refer to the appendix section.

In designing the sensing matrix we would like to minimize the number of measurement needed to recover  $\Sigma$ . We also need the message-passing algorithm to converge, in other words  $V^{(t)} \rightarrow 0$  and the average error should shrink to zero,  $E^{(t)} \rightarrow 0$  as  $t \rightarrow \infty$ . However, enforcing  $\lim_{t \rightarrow \infty} (E^{(t)}, V^{(t)}) = (0, 0)$  is not straightforward and it requires running the DE updates numerically until convergence is achieved. For the case of sparse vector recovery, (Zhang et al.) showed that these requirements can be reduced to two inequality constraints making it easier to check for satisfiability. We extend this to case of covariance recovery in the form of the following theorem.

**Theorem 3.1.** *Let  $\Sigma$  be  $k^2$ -sparse and set  $\beta$  to be  $p^2 / (c_0 \log(p/k))$  for  $c_0 > 0$ . Then, the necessary condition for  $\lim_{t \rightarrow \infty} (E^{(t)}, V^{(t)}) = (0, 0)$  results in  $a_1^2 \leq p^2 / k^2$  and  $a_2 \leq p^2 / (2c_0 k^2 \log(p/k))$ , where  $a_1 = \sum_{i,i',j,j'} \rho_i \rho_{i'} \lambda_j \lambda_{j'} \sqrt{i i' / j j'}$  and  $a_2 = \sum_{i,i',j,j'} \rho_i \rho_{i'} \lambda_j \lambda_{j'} (i i' / j j')$ .*

Therefore the design of the sensing matrix can be posed as the following optimization problem,

$$\min_{\substack{\lambda \in \Delta_{d_v} \\ \rho \in \Delta_{d_c}}} \frac{d}{p} = \frac{\sum_{i \geq 2} i \lambda_i}{\sum_{j \geq 2} \rho_j} \quad (12)$$

$$\text{s.t. } a_1^2 \leq \frac{p^2}{k^2} \quad (13)$$

$$a_2 \leq \frac{p^2}{2c_0 k^2 \log(p/k)} \quad (14)$$

$$\lambda_1 = \rho_1 = 0, \quad (15)$$

where  $\Delta_d$  is a  $d$ -dimensional simplex,  $d_v$  and  $d_c$  denote the maximum column and row degree respectively of sensing matrix  $\mathbf{A}$ . The final constraint (15) is added to avoid

one-way message passing. Once we have the distributions  $\lambda$  and  $\rho$  we then sample the sensing matrix such that the number of non-zero entries in the rows and columns satisfy the obtained distributions. For every non-zero entry of  $\mathbf{A}$ ,  $P(A_{ij} = A^{-1/2}) = P(A_{ij} = -A^{-1/2}) = \frac{1}{2}$ . With the sensing matrix obtained,  $(\mathbf{P}_2)$  can be solved using any convex program solver.

## 4. Graph Structure Recovery

In this section, we discuss the steps involved in the recovery of the underlying structure of the GBN. (Ghoshal & Honorio, 2017) showed that the structure of GBN can be recovered using the covariance and the precision matrix of the joint distribution of  $X_1, \dots, X_p$ . Once the covariance matrix is retrieved as discussed in the previous section, the precision matrix is obtained using *Constrained  $\ell_1$ -minimization for Inverse Matrix Estimation* (CLIME), a constrained convex optimization framework, proposed by (Cai et al., 2011). CLIME forces the precision matrix to approximate the inverse of the estimated covariance matrix by minimizing  $\|\hat{\Sigma}\Theta - \mathbf{I}\|_\infty$ . Using the estimated covariance and precision matrix, the following steps are performed to obtain the structure of the GBN:

1. Identify the Markov blanket of each node ( $MB_i$ ). This is done by looking at indices of the non-zero entries of each column/row of the precision matrix  $\Omega$ .
2. Compute the regression coefficients ( $\theta_i$ ), which depends on covariance matrix and the markov blankets. The regression coefficients are defined as,

$$\theta_i^T \mathbf{x}_{-i} = \mathbf{E}[X_i | X_{-i} = \mathbf{x}_{-i}].$$

3. Identify the terminal nodes, which depends on the precision matrix  $\Omega$  and regression coefficients  $\theta_i$ . Let us define,  $r_i = \max_{j \in MB_i} \left| \frac{\Omega_{ij}}{\theta_{ij}} \right|$ . Then  $v = \arg \min_i r_i$  is the terminal node. Once we have the terminal node, the markov blanket gives the parents of the terminal node.
4. The terminal node is removed and the joint distribution is marginalized with respect to the terminal node.

These four steps are repeated until only one node is left in the graph providing us with all the parent-child relations in the graph and thereby the structure of the Bayesian network.

## 5. Experiments

In this section we present the numerical experiments performed on the recovery system. To generate the GBN, we

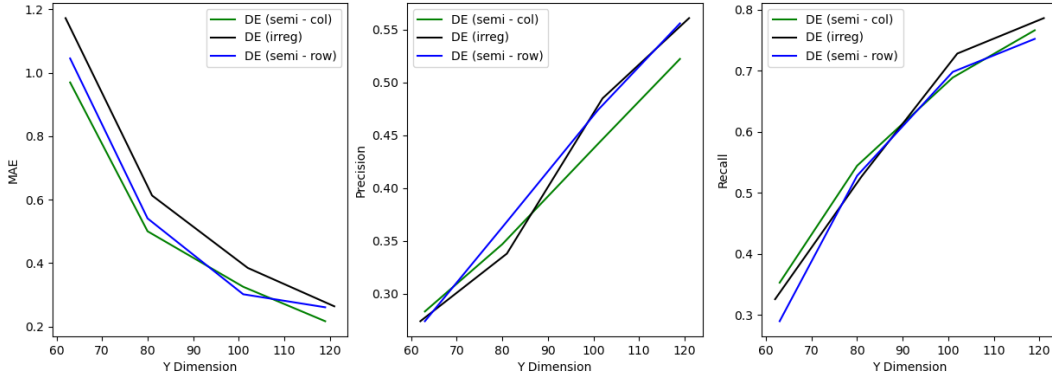


Figure 4. Comparison of performance of the three sensing systems for recovery covariance matrix. *Semi - col* denotes Fixed column degree and variable row degree, *semi - row* denotes fixed row degree and variable column degree, and finally *irregular* denotes variable row and column degree. The reconstruction performance is evaluated with respect to *Maximum Absolute Error (MAE)*, *Precision* of the support of the covariance matrix, *Recall* of the support of the covariance matrix. The figure shows performance when the number of nodes in the graph  $p = 200$ .

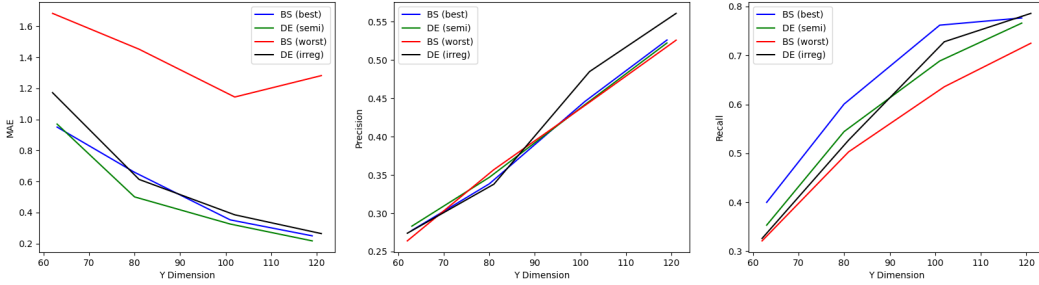


Figure 5. Comparison of the performance of the proposed sensing systems with the state of the sensing systems proposed by (Dasarathy et al., 2015), denoted as BS in the plots. For the baseline, we chose two different versions of the sensing system, one where there hyperparameters are tuned (BS - best) and one where the parameters were initialized randomly (BS - worst). The figure shows the performance when the number of nodes in the graph  $p = 200$ .

sampled directed graphs from Erdős-Renyi class of random graphs with edge weights set to  $\pm 1/2$  with probability  $1/2$ . We first study the effectiveness of the sensing system for covariance recovery and consider three different design schemes: (1) fix the row degree and solve for the column degrees, (2) fix the column degree fixed and solve for the row degree, and (3) solve for both the row degree and the column degree. We also compare the performance with the current state of the art. We then evaluate the performance of the sensing system for graph structure recovery.

### 5.1. Covariance Recovery

As mentioned earlier, we consider three different design schemes for constructing the sensing matrix.

1. *Fixed row degree and variable column degree.* In this case,  $\rho_i = 1$  when  $i = d_c$  and 0 otherwise. We then solve (12) for  $\lambda$ .
2. *Fixed column degree and variable row degree.* In this case,  $\lambda_i = 1$  when  $i = d_v$  and 0 otherwise. We then solve (12) for  $\rho$ .
3. *Variable row and column degree.* In this case we solve (12) for both  $\lambda$  and  $\rho$ .

In case (1) and (2), the resulting optimization program is readily solvable by any convex program solver. For case (3), we first keep  $\lambda$  constant and solve for  $\rho$ , then using the obtained solution for  $\rho$  we solve for  $\lambda$ .

The recovery performance is evaluated using three metrics,

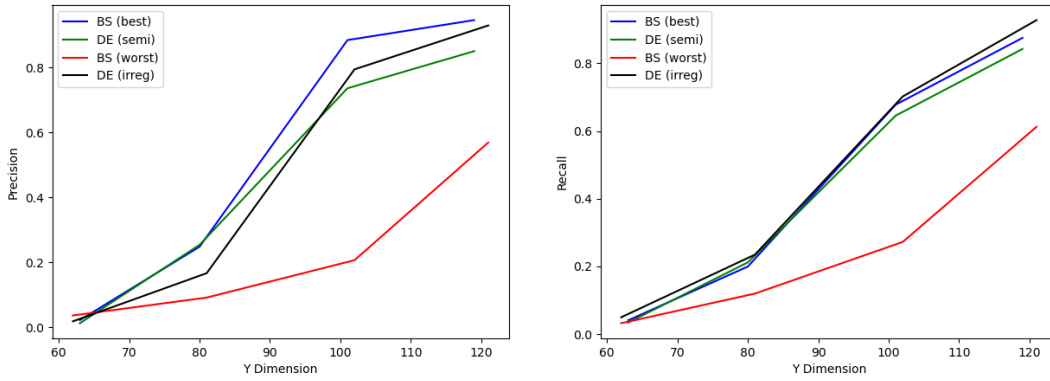


Figure 6. Comparison of the performance of the proposed sensing system with that of (Dasarathy et al., 2015) (BS - best, BS - worst, lines in the plots). Number of nodes,  $p = 100$ . The performance is evaluated with respect to *precision* and *recall* of the edges in the graph.

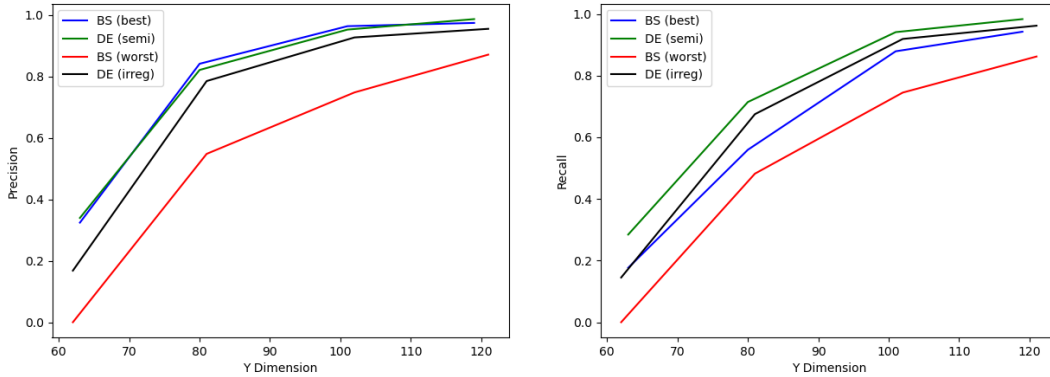


Figure 7. Comparison of the performance of the proposed sensing system with that of (Dasarathy et al., 2015) (BS - best, BS - worst lines in the plots). Number of nodes,  $p = 200$ . The performance is evaluated with respect to *precision* and *recall* of the edges in the graph.

namely, (1) *Maximum Absolute Error* (MAE) which is given by the maximum absolute difference between the estimate covariance matrix and the ground truth covariance matrix, (2) *Precision* of the recovery of the support of the covariance matrix, since the covariance is sparse we measure the percentage of estimated support that belongs to the support of the ground truth covariance, and (3) *Recall* which measures the percentage of the support of the ground truth covariance that has been recovered.

First, we compare the relative performance between the three design schemes. In Figure 4 we can see that the performance is very similar across the different design schemes with some small fluctuations, hence there isn't any inherent advantage of choosing one over the other. We also compare the performance of our sensing system to the one proposed by (Dasarathy et al., 2015), Figure 5, where the sensing

matrix is taken to be the adjacency matrix of a  $\delta$ -left regular bipartite graph and  $\delta$  is a parameter that has to be tuned. In this case, for the density evolution based design we consider cases (2) and (3). As seen from the figure, density evolution based sensing matrices achieve similar performance to that (Dasarathy et al., 2015) when  $\delta$  is tuned. On the other hand, improper assignment of  $\delta$  results in poor performance compared to the density evolution based design.

At this point, we also point out that in order to generate the sensing matrix, it is sufficient to choose  $d_v$  and  $d_c$  such that 12 is feasible. Hence, it doesn't involve a lot of tuning. Therefore, unlike (Dasarathy et al., 2015) our approach is more scalable as tuning  $\delta$  can sometimes take considerable effort and requires ground truth data.

Additionally, the sensing matrices obtained from our design

scheme can be thought of extensions of (Dasarathy et al., 2015) as in their case they keep the column degree fixed but do not impose any constraint on the row degrees. Where as in our approach we solve for the optimum degree for the rows of  $A$ . Moreover, in design schemes (1) and (3) the column degrees are variable, not considered by (Dasarathy et al., 2015).

## 5.2. Graph Recovery

From the covariance matrix we recovered from the observations  $\mathbf{y}$ , CLIME (Cai et al., 2011) is used to estimate the precision matrix. Using the covariance and the precision matrix, the graph structure, the support of weighted adjacency matrix ( $\mathbf{W}$ ), is recovered as described in section 4. The performance is evaluated using precision and recall as metrics, where precision measures the percentage of the correct edges predicted versus the total predicted edges and recall measures the percent of the original edges that are correctly predicted.

Figures 6 and 7 shows the performance comparison when the number of nodes in the graph  $p = 100$  and  $p = 200$  respectively. For the proposed framework we compare the performance of design schemes (2) and (3). For the state of the art sensing system, (Dasarathy et al., 2015), we again choose two values for  $\delta$ , (BS - best) corresponds to  $\delta$  with ground truth data and (BS - worst) corresponds to randomly assigned  $\delta$ . A similar trend to covariance recovery is observed, the proposed sensing systems are capable of matching the performance of when  $\delta$  is tuned. The simulations also establish that the graph structure can indeed be recovered from compressed measurements. We even obtain close to perfect recovery when  $\mathbf{y}$  dimension ( $d$ ) is 60 (60% of the original size) for  $p = 100$  and when  $\mathbf{y}$  dimension ( $d$ ) is 90 (45% of the original size) for  $p = 200$ . We can also see that more compression can be achieved when  $p$  becomes large as evident from the two figures, higher precision and recall values are attained for lower  $d/p$  ratio when  $p = 200$ .

Since the graph structure recovery relies on covariance matrix, the trade-offs of covariance recovery still apply here. That is, for obtaining best  $\delta$ , tuning still has to be performed as explained in the previous subsection and hence the same pitfalls for (Dasarathy et al., 2015) would still hold.

## 6. Conclusion

In this paper, we presented a general framework for collecting lower dimensional samples of signal generated from a GBN for accurate recovery of the graph structure. We also showcased the feasibility of our approach through numerical simulations. There are several directions that could be of interest in the future. While we restricted our focus to GBNs, exploring other types of additive noise distributions would

be an interesting avenue. The proposed density evolution framework can also be extended to design sensing systems for preferential sensing of certain nodes in the graph.

## References

- Berinde, R., Gilbert, A. C., Indyk, P., Karloff, H., and Strauss, M. J. Combining geometry and combinatorics: A unified approach to sparse signal recovery. In *2008 46th Annual Allerton Conference on Communication, Control, and Computing*, pp. 798–805. IEEE, 2008.
- Cai, T., Liu, W., and Luo, X. A constrained  $\ell_1$  minimization approach to sparse precision matrix estimation. *Journal of the American Statistical Association*, 106(494):594–607, 2011.
- Candes, E., Romberg, J., and Tao, T. Robust uncertainty principles: exact signal reconstruction from highly incomplete frequency information. *IEEE Transactions on Information Theory*, 52(2):489–509, 2006. doi: 10.1109/TIT.2005.862083.
- Chickering, M., Heckerman, D., and Meek, C. Large-sample learning of bayesian networks is np-hard. *Journal of Machine Learning Research*, 5, 2004.
- Dasarathy, G., Shah, P., Bhaskar, B. N., and Nowak, R. D. Sketching sparse matrices, covariances, and graphs via tensor products. *IEEE Transactions on Information Theory*, 61(3):1373–1388, 2015. doi: 10.1109/TIT.2015.2391251.
- DeVore, R. A. Deterministic constructions of compressed sensing matrices. *Journal of complexity*, 23(4-6):918–925, 2007.
- Donoho, D. L., Maleki, A., and Montanari, A. Message-passing algorithms for compressed sensing. *Proceedings of the National Academy of Sciences*, 106(45):18914–18919, 2009.
- Gallager, R. Low-density parity-check codes. *IRE Transactions on Information Theory*, 8(1):21–28, 1962. doi: 10.1109/TIT.1962.1057683.
- Ghoshal, A. and Honorio, J. Learning identifiable gaussian bayesian networks in polynomial time and sample complexity. In Guyon, I., Luxburg, U. V., Bengio, S., Wallach, H., Fergus, R., Vishwanathan, S., and Garnett, R. (eds.), *Advances in Neural Information Processing Systems*, volume 30. Curran Associates, Inc., 2017. URL <https://proceedings.neurips.cc/paper/2017/file/907edb0aa6986220dbfffb79a788596ee-Paper.pdf>.



- Guo, R., Cheng, L., Li, J., Hahn, P. R., and Liu, H. A survey of learning causality with data: Problems and methods. *ACM Computing Surveys (CSUR)*, 53(4):1–37, 2020.
- Kaplan, A., Pohl, V., and Lee, D. G. On compressive sensing of sparse covariance matrices using deterministic sensing matrices. In *2018 IEEE International Conference on Acoustics, Speech and Signal Processing (ICASSP)*, pp. 4019–4023. IEEE, 2018.
- Krzakala, F., Mézard, M., Sausset, F., Sun, Y., and Zdeborová, L. Statistical-physics-based reconstruction in compressed sensing. *Physical Review X*, 2(2):021005, 2012a.
- Krzakala, F., Mézard, M., Sausset, F., Sun, Y., and Zdeborová, L. Probabilistic reconstruction in compressed sensing: algorithms, phase diagrams, and threshold achieving matrices. *Journal of Statistical Mechanics: Theory and Experiment*, 2012(08):P08009, 2012b.
- Mezard, M. and Montanari, A. *Information, physics, and computation*. Oxford University Press, 2009.
- Müller, J., Kuttler, C., and Hense, B. A. Sensitivity of the quorum sensing system is achieved by low pass filtering. *Biosystems*, 92(1):76–81, 2008.
- Pearl, J. *Probabilistic reasoning in intelligent systems: networks of plausible inference*. Morgan kaufmann, 1988.
- Spirtes, P., Glymour, C. N., Scheines, R., and Heckerman, D. *Causation, prediction, and search*. MIT press, 2000.
- Van de Geer, S. and Bühlmann, P.  $\ell_0$ -penalized maximum likelihood for sparse directed acyclic graphs. *The Annals of Statistics*, 41(2):536–567, 2013.
- Zdeborová, L. and Krzakala, F. Statistical physics of inference: Thresholds and algorithms. *Advances in Physics*, 65(5):453–552, 2016.
- Zhang, H., Abdi, A., and Fekri, F. A general framework for the design of compressive sensing using density evolution. In *IEEE Information Theory Workshop (ITW'21)*.
- Zheng, X., Aragam, B., Ravikumar, P. K., and Xing, E. P. Dags with no tears: Continuous optimization for structure learning. In Bengio, S., Wallach, H., Larochelle, H., Grauman, K., Cesa-Bianchi, N., and Garnett, R. (eds.), *Advances in Neural Information Processing Systems*, volume 31. Curran Associates, Inc., 2018. URL <https://proceedings.neurips.cc/paper/2018/file/e347c51419ffb23ca3fd5050202f9c3d-Paper.pdf>.

## A. Degree Distribution of Check nodes and Variable nodes

As described in section 3.1, let  $\lambda \in \Delta_{d_v}$ ,  $\rho \in \Delta_{d_c}$  be the degree distributions of columns and rows of  $\mathbf{A}$ . We can divide  $\gamma$  and  $\chi$  into blocks of size  $d$  and  $p$  nodes respectively. Each block corresponds to a column of  $\Sigma_Y$  and  $\Sigma$ . Let  $\gamma_i$  denote the  $i$ -th block of  $\gamma$  and similarly let  $\chi_j$  denote the  $j$ -th block of  $\chi$ . In the factor graph, 3, blocks  $\gamma_i$  and  $\chi_j$  are connected if at least one node in  $\gamma_i$  is connected to at least one node in  $\chi_j$ . The connections at the block level are defined by the sensing matrix  $\mathbf{A}$ . In other words,  $\gamma_i$  and  $\chi_j$  are connected if  $A_{ij} \neq 0$ . Figure 8, illustrates the connections at the block level.

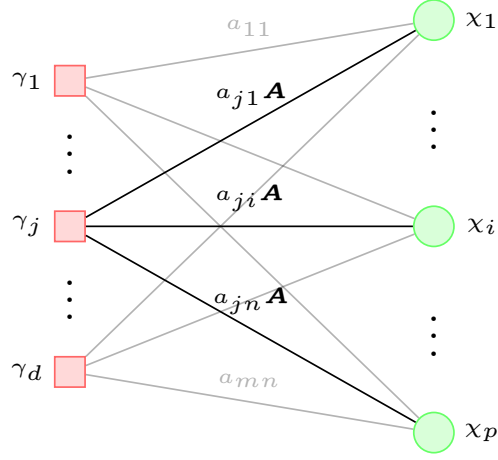


Figure 8. Illustration of the connections in the factor graph at block level.

Let us now focus on the connections between the nodes in block  $\gamma_j$  and  $\chi_i$ . We denote  $\gamma_j^{(k)}$  to be the  $k$ -th node in check node block  $j$  and  $\chi_i^\ell$  to be the  $\ell$ -th node in the variable node block  $i$ . The connections between the blocks  $\gamma_j$  and  $\chi_i$ , if it exists ( $A_{ji} \neq 0$ ), is again characterized by  $\mathbf{A}$ . Figure 9 illustrated the connected between the nodes in a variable node block and a check node block.

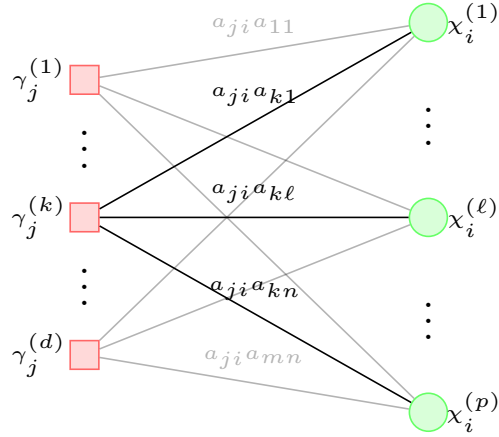


Figure 9. Illustration of the connections between blocks  $\gamma_j$  and  $\chi_i$

Therefore we now have,

$$\gamma_j^{(k)} = \sum_{i=1}^p \sum_{\ell=1}^p A_{ji} A_{k\ell} \chi_i^{(\ell)}. \quad (16)$$

Since  $\deg(\gamma_j^{(k)})$  would be the number of non-zero terms in the above summation, we then have  $\deg(\gamma_j^{(k)}) = \deg(A^{(j)}) \deg(A^{(k)})$ , where  $A^{(j)}$  denotes the  $j$ -th row of  $\mathbf{A}$ . Using a similar argument we can also conclude that  $\deg(\chi_i^{(\ell)}) =$

$\deg(A_i)\deg(A_\ell)$ , where  $A_i$  denotes the  $i$ -th column of  $\mathbf{A}$ . Since  $\deg(A_i) \in \{1, \dots, d_v\}$  and  $\deg(A^{(j)}) \in \{1, \dots, d_c\}$  we have that  $\deg(\gamma_j^{(k)}) \in \{1, \dots, d_c^2\}$  and  $\deg(\chi_i^{(\ell)}) = \{1, \dots, d_v^2\}$ . Therefore we have

$$P\left(\deg(\gamma_j^{(k)}) = k\right) = \sum_{j,j':jj'=k} \rho_j \rho_{j'} \quad (17)$$

And,

$$P\left(\deg(\chi_i^{(\ell)}) = k\right) = \sum_{i,i':ii'=k} \lambda_i \lambda_{i'} \quad (18)$$

## B. Derivation of DE Update Equations

As described in section 3, in order to analyze the convergence of the message-passing algorithm, the two quantities given by equations (8) and (9) are tracked over the course of the algorithm, re-written here for convenience.

$$E^{(t)} = \frac{1}{d^2 p^2} \sum_{a=1}^{d^2} \sum_{i=1}^{p^2} \left( \mu_{i \rightarrow a}^{(t)} - \chi_i^* \right)^2;$$

$$V^{(t)} = \frac{1}{d^2 p^2} \sum_{a=1}^{d^2} \sum_{i=1}^{p^2} v_{i \rightarrow a}^{(t)}.$$

To simplify these two quantities, we need to simplify the messages flowing through the factor graph. To that end, we start with the messages sent from the check nodes to the variable nodes,  $\hat{m}_{a \rightarrow i}^{(t)} \sim \mathcal{N}\left(\hat{\mu}_{a \rightarrow i}^{(t)}, \hat{v}_{a \rightarrow i}^{(t)}\right)$ . (Zhang et al.) derived a simplified update for the  $\hat{\mu}_{a \rightarrow i}^{(t)}$  and  $\hat{v}_{a \rightarrow i}^{(t)}$  in Lemma 6. Here we list the lemma and modify it our purpose to account for the Kronecker product sensing matrix.

**Lemma B.1.** Consider the message flowing from check node  $a$  to variable node  $i$ ,  $\hat{m}_{a \rightarrow i}^{(t)} \sim \mathcal{N}\left(\hat{\mu}_{a \rightarrow i}^{(t)}, \hat{v}_{a \rightarrow i}^{(t)}\right)$ . Then the following update can be obtained at the  $(t+1)$ -th iteration.

$$\hat{\mu}_{a \rightarrow i}^{(t+1)} = \chi_i + A \sum_{j \in \partial a \setminus i} A_{ai}^{\otimes} A_{aj}^{\otimes} \left( \chi_j - \mu_{j \rightarrow a}^{(t)} \right) + A A_{ai}^{\otimes} n_a; \quad (19)$$

$$\hat{v}_{a \rightarrow i}^{(t+1)} = A \sigma^2 + |\partial a| V^{(t)}. \quad (20)$$

Where  $\chi_i$  is the  $i$ -th variable node and  $|\partial a|$  is the degree of the check node  $a$ .

Now consider the message going from variable nodes to check nodes,  $m_{i \rightarrow a}^{(t)} \sim \mathcal{N}\left(\mu_{i \rightarrow a}^{(t)}, v_{i \rightarrow a}^{(t)}\right)$ . Using the previous lemma and exploiting some properties of Gaussian distribution with some approximations along the way,  $\mu_{i \rightarrow a}^{(t)}$  and  $v_{i \rightarrow a}^{(t)}$  can be updated as follows, here we also make use of the characterization of degrees of check nodes and the variable nodes from the section A. The readers are referred to (Zhang et al.) for more details.

$$\mu_{i \rightarrow a}^{(t+1)} \approx h_{\text{mean}} \left( \chi_i + z \sum_{i,i',j,j'} \rho_i \rho_{i'} \lambda_j \lambda_{j'} \sqrt{\frac{ii' E^{(t)} + A \sigma^2}{jj'}}; \sum_{i,i',j,j'} \rho_i \rho_{i'} \lambda_j \lambda_{j'} \frac{ii' E^{(t)} + A \sigma^2}{jj'} \right); \quad (21)$$

$$v_{i \rightarrow a}^{(t+1)} \approx h_{\text{var}} \left( \chi_i + z \sum_{i,i',j,j'} \rho_i \rho_{i'} \lambda_j \lambda_{j'} \sqrt{\frac{ii' E^{(t)} + A \sigma^2}{jj'}}; \sum_{i,i',j,j'} \rho_i \rho_{i'} \lambda_j \lambda_{j'} \frac{ii' E^{(t)} + A \sigma^2}{jj'} \right). \quad (22)$$

Where  $h_{\text{mean}}$  and  $h_{\text{var}}$  are given by,

$$h_{\text{mean}}(\mu; v) = \lim_{\beta \rightarrow \infty} \frac{\int x_i e^{-\beta f(x_i)} e^{-\frac{\beta(x_i - \mu)^2}{2v}} dx_i}{\int e^{-\beta f(x_i)} e^{-\frac{\beta(x_i - \mu)^2}{2v}} dx_i}; \quad h_{\text{var}}(\mu; v) = \lim_{\beta \rightarrow \infty} \frac{\int x_i^2 e^{-\beta f(x_i)} e^{-\frac{\beta(x_i - \mu)^2}{2v}} dx_i}{\int e^{-\beta f(x_i)} e^{-\frac{\beta(x_i - \mu)^2}{2v}} dx_i} - h_{\text{mean}}(\mu; v)$$

By plugging equations (21) and (22) in (8) and (9) yields the following,

$$E^{(t+1)} = \mathbf{E}_{\text{prior}(s)} \mathbf{E}_z \left[ h_{\text{mean}} \left( s + z \sum_{i,i',j,j'} \rho_i \rho_{i'} \lambda_j \lambda_{j'} \sqrt{\frac{ii' E^{(t)} + A\sigma^2}{jj'}}; \sum_{i,i',j,j'} \rho_i \rho_{i'} \lambda_j \lambda_{j'} \frac{ii' E^{(t)} + A\sigma^2}{jj'} \right) - s \right]^2; \quad (23)$$

$$V^{(t+1)} = \mathbf{E}_{\text{prior}(s)} \mathbf{E}_z h_{\text{var}} \left( s + z \sum_{i,i',j,j'} \rho_i \rho_{i'} \lambda_j \lambda_{j'} \sqrt{\frac{ii' E^{(t)} + A\sigma^2}{jj'}}; \sum_{i,i',j,j'} \rho_i \rho_{i'} \lambda_j \lambda_{j'} \frac{ii' E^{(t)} + A\sigma^2}{jj'} \right). \quad (24)$$

By setting  $f(\chi) = \beta \|\chi\|_1$ , we enforce the returned solutions to be sparse. This is equivalent to choosing Laplacian prior for  $\chi$ . Following (Donoho et al., 2009) in the noiseless case, equations (23) and (24) reduce to equations (10) and (11).

### C. Relaxation of Message-passing convergence constraint

In this section we sketch the proof of Theorem 3.1, refer to (Zhang et al.) for more details of the proof. The derivation of necessary conditions for  $\lim_{t \rightarrow \infty} (E^{(t)}, V^{(t)}) = (0, 0)$  can be split into two parts:

- **Part 1.** Showing that  $(0, 0)$  is a fixed point of the DE update equation.
- **Part 2.** Necessary conditions for DE update equations to converge in the neighborhood of  $(0, 0)$ .

By substituting  $(E^{(t)}, V^{(t)}) = (0, 0)$  we can see that it is indeed a fixed point. We begin part 2 by analyzing the functions  $\delta_E^{(t)} = E^{(t+1)} - E^{(t)}$  and  $\delta_V^{(t)} = V^{(t+1)} - V^{(t)}$ . Let us define the functions  $\Psi_E$  and  $\Psi_V$  as follows,

$$\begin{aligned} \Psi_E(E^{(t)}; V^{(t)}) &= \mathbf{E}_{\text{prior}(s)} \mathbf{E}_{z \sim \mathcal{N}(0,1)} \left[ \text{prox} \left( s + a_1 z \sqrt{E^{(t)}}; \beta a_2 V^{(t)} \right) - s \right]^2; \\ \Psi_V(E^{(t)}; V^{(t)}) &= \mathbf{E}_{\text{prior}(s)} \mathbf{E}_{z \sim \mathcal{N}(0,1)} \left[ \beta a_2 V^{(t)} \text{prox}' \left( s + a_1 z \sqrt{E^{(t)}}; \beta a_2 V^{(t)} \right) \right]^2. \end{aligned}$$

By taking the Taylor expansion of  $\delta_E^{(t+1)}$  and  $\delta_V^{(t+1)}$  and dropping the higher order terms we obtain,

$$\begin{bmatrix} \delta_E^{(t+1)} \\ \delta_V^{(t+1)} \end{bmatrix} = \underbrace{\begin{bmatrix} \left( \frac{\partial \Psi_E(E, V)}{\partial E} \right)^{(t)} & \left( \frac{\partial \Psi_E(E, V)}{\partial V} \right)^{(t)} \\ \left( \frac{\partial \Psi_V(E, V)}{\partial E} \right)^{(t)} & \left( \frac{\partial \Psi_V(E, V)}{\partial V} \right)^{(t)} \end{bmatrix}}_{=: \mathbf{L}^{(t)}} \begin{bmatrix} \delta_E^{(t)} \\ \delta_V^{(t)} \end{bmatrix}$$

For  $\Psi_E$  and  $\Psi_V$  to converge to 0, we would want the operator norm of  $\mathbf{L}^{(t)}$  to be less than 1, i.e.,  $\inf_t \|\mathbf{L}^{(t)}\| \leq 1$ . Since

$$\|\mathbf{L}^{(t)}\| = \max \left[ \left( \frac{\partial \Psi_E(E, V)}{\partial E} \right)^{(t)}, \left( \frac{\partial \Psi_V(E, V)}{\partial V} \right)^{(t)} \right].$$

We can restrict the lower bounds of the individual terms to be less than 1. This would result in

$$a_1^2 \leq \frac{p^2}{k^2}, \quad a_2 \leq \frac{p^2}{k^2 \beta}.$$